Effect of zinc injection timing on the characterization of oxide film of Alloy 690TT in simulated PWR primary coolant

Dong-Seok Lim[a,b], Soon-Hyeok Jeon[a], Jong-Hyeon Lee[b], Jinsoo Choi[c], Kyu Min Song[c], Do Haeng Hur[a,*]

[a]*Materials Safety Technology Development Division, Korea Atomic Energy Research Institute, 989-111, Daedeok-daero, Yuseong-gu, Daejeon, 34057, Republic of Korea*
[b]*Department of Materials Science and Engineering, Chungnam National University, 99, Daehak-ro, Yuseong-gu, Daejeon, 34134, Republic of Korea*
[c]*Central Research Institute of Korea Hydro & Nuclear Power Co., Ltd, 1312-70, Yuseong-daero, Yuseong-gu, Daejeon, Republic of Korea*

[*]*Corresponding author:dhhur@kaeri.re.kr*

1. Introduction

In the primary water system of pressurized water reactors (PWRs), Co-58 and Co-60 are known as the major sources of the radiation field and produced by a radioactivation of Ni-58 and Co-59, respectively. Corrosion products such as Fe, Ni, and Co are mainly released from steam generator (SG) tubes exposed to primary coolant water. Consequently, the corrosion products are transported by the primary coolant and deposited on the surfaces of fuel claddings. The activated corrosion products in the core are the major source of radiation build-up and occupational radiation exposure of workers during shutdown maintenance period [1,2].

In order to reduce the radiation field, the corrosion products released from SG tubes should be minimized because the SG tubes occupy over 65% of the total surface area exposed to the primary coolant of PWRs. Thus, it is important to evaluate and mitigate general corrosion of the SG tubes [3,4].

In previous studies, the general corrosion rate of Alloy 690 SG tubes was affected by various water chemistry parameters such as dissolved oxygen (DO), dissolved hydrogen (DH), temperature, and pH value. Furthermore, zinc addition has also been performed as an important method to minimize the radiation field and general corrosion rate. In most of nuclear power plants, zinc is added to the primary water with a concentration of 5 to 10 ppb according to the EPRI guideline [5-8]. There are a few investigations on the effects of zinc injection timing on the general corrosion behavior of SG tubes in primary water condition of PWRs.

However, the degree of the general corrosion due to the variation in the characteristics of the oxide film by the zinc injection timing still remains unquantified. Therefore, in this study, the effects of four zinc injection timing on the oxide formation behavior of Alloy 690TT were investigated using a primary loop system. The microstructure of the oxide films of Alloy 690TT was analyzed by scanning electron microscope (SEM), transmission electron microscopy (TEM), and energy dispersed spectroscopy (EDS). Based on the characterization of the oxide films, we discussed about the general corrosion behavior of Alloy 690TT and optimal zinc injection timing.

2. Experimental methods

2.1 Specimen and solution preparation

The tubing material used in this work was Alloy 690TT with an outer diameter of 19.07 mm and a wall thickness of 1.07 mm. The chemical composition of the Alloy 690TT SG tube is presented in Table I. Tubular specimens were prepared with a size of 50 mm in length by cutting the long tubing material transversely for corrosion tests. The corrosion specimens have a hole of 3 mm in diameter in order to hang on a specimen tree in the autoclave for high-temperature corrosion tests. Some part of SG tubes were cut into 4 mm x 12 mm x 1.07 mm for an oxide film analysis.

The simulated primary coolant of PWR was prepared by high purity demineralized distilled water with the resistivity above 18 MΩ-cm and nuclear-grade lithium hydroxide (LiOH) and boric acid (H_3BO_3). The test solution contained 2 ppm Li, and 1000 ppm B. In addition, depleted zinc acetate (DZA), which is widely used in PWRs, was added to the primary coolant for control the zinc concentration. DO was controlled to be less than 5 ppb and DH was maintained 35 cc/kg by controlling the hydrogen overpressure of the solution tank. Corrosion tests were performed at 330 °C under 150 bar.

Table I. Chemical composition of Alloy 690TT (wt. %).

C	Si	Al	Ti	Mn	Fe	Cr	Ni
0.02	0.30	0.14	0.16	0.29	10.1	29.3	59.6

2.2 Corrosion tests

Fig. 1 presents the schematic of the primary water recirculating system used for the corrosion tests. The loop system consisted of the following main components: solution tank of primary water, high pressure (HP) pump, pre-heater, heat exchanger, back pressure regulator (BPR), various water chemistry sensors such as DO, pH, and conductivity sensors.

The simulated primary water in the solution tank was recirculated through the HP pump, pre-heater, test section and heat exchanger. During the corrosion tests, Two tanks (200 L and 100 L capacity) were used and switched each other to maintain the target zinc concentration. 200 L and 100 L tanks were used for 10 and 5 days, respectively.

Table II shows the four zinc injection timing conditions for the corrosion tests. At case 1, zinc was continuously injected to the primary water until the finish of the corrosion test for 3000 h. In the case 2, zinc was not injected to the coolant until the finish of the test for 3000 h. During the performing the test for 3000 h, zinc was firstly injected to the coolant for 1500 h, and the corrosion test was performed without zinc injection for 1500 h (case 3). On the contrary to the case 3, in the case 4, zinc was not injected to the primary water for 1500 h, and the corrosion test was conducted with zinc injection for 1500 h. Under these four zinc injection conditions, the corrosion tests were performed in simulated primary water at 330 °C.
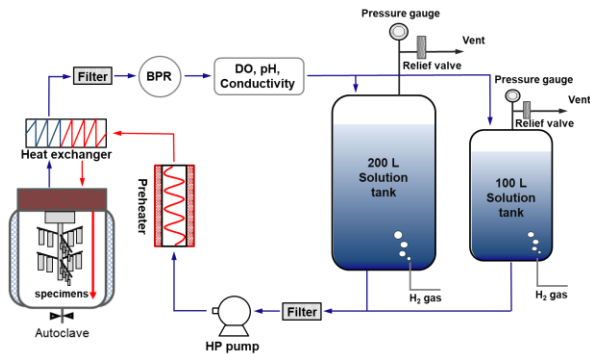
Fig. 1. Schematic diagram of loop system for general corrosion test.

Table II. Four zinc injection conditions for general corrosion test.

	Zn injection conditions	
	Stage 1 (1500 h)	Stage 2 (1500 h)
Case 1	O	O
Case 2	X	X
Case 3	O	X
Case 4	X	O

O: Zn injection, X: no Zn injection

2.3 Microstructural characterization

After the corrosion tests, the morphology of oxide films formed on Alloy 690 specimens was observed using SEM. The focus ion beam (FIB) milling technique was used to prepare TEM samples, allowing us to produce samples of which the oxide film structure could be observed in depth. The oxide properties were analyzed using TEM and TEM- energy dispersive X-ray spectroscopy (EDS).

3. Results and Discussion

Fig. 2 shows the SEM micrographs of the oxide films formed on Alloy 690 surface after 3000 h corrosion test under the four different zinc injection timing. All specimens had polyhedral-shaped oxide particles. As shown in Fig. 2(a), the surface of Alloy 690 was covered with numerous small polyhedral particles (50 ~ 200 nm) at case 1. However, oxide particles were not observed on most surface of Alloy 690. As shown in Fig. 2 (b) and (d), the both specimens were mainly covered with small polyhedral particles with a size of 50 ~ 200 nm and rel atively large polyhedral particles with a size of 1 ~ 2 μm. However, the size of polyhedral particle oxides in Fig. 2(b) were slightly larger than that of polyhedral particle oxides in Fig. 2(d). In Fig. 2(c), two types of oxide particles such as the rod-like and polyhedral particles were formed on the surface of Alloy 690TT. Based on the SEM results, it is concluded that the surface morphologies and particles size of oxide film were significantly changed with zinc injection conditions.

Furthermore, when zinc was firstly injected to the coolant for 1500 h (cases 1 and 3), it could be also observed that the size of the oxide particles formed on the outermost layer is relatively smaller than those of cases 2 and 4. These phenomena could be explained by the substitution reaction of zinc to oxide and its superior stability. The oxides containing zinc are more thermodynamically stable than the zinc-free oxide. Stable oxides mean that it is difficult for oxide to dissolve and precipitate. However, the growth of outermost layers of nickel-based alloys is greatly controlled by dissolution and precipitation of Fe or Ni oxides. Hence, in cases 1 and 3, the stable oxide containing zinc initially formed and the growth of the oxide formed on the outermost layer was suppressed.
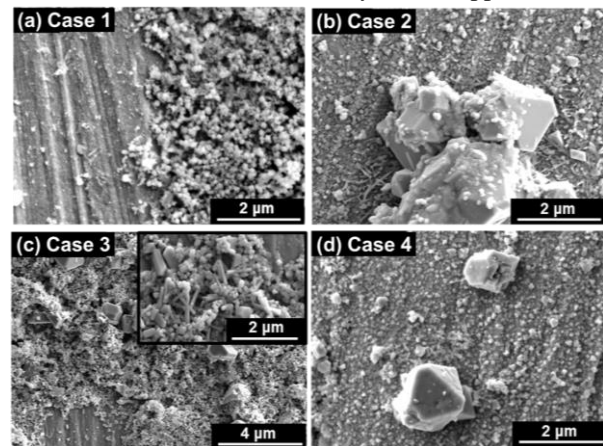
Fig. 2. SEM micrographs of surface of oxide films formed on Alloy 690TT after corrosion tests for 3000 h under the four zinc injection conditions: (a) case 1, (b) case 2 , (c) case 3, and (d) case 4.

Fig. 3 shows the TEM images and line EDS scan analysis of the cross section of oxide films formed on Alloy 690TT. As shown in Fig. 3(a), the outmost particle was composed of Fe-rich oxide layer with Cr, Ni and Zn. The inner layer was composed of Cr-rich oxide containing Zn, Ni, and Fe. Point EDS of oxide particles is presented in Table III. In Fig. 3(b) and Table III, the polyhedral particles were composed of Fe-rich oxide with Ni and Cr. As shown in Fig 3(c), the relatively large polyhedral particle was composed Fe-rich oxide with Ni. At Table III (point 4), the needle-like particle was composed of Zn-rich oxide with Fe and Ni. In the case of (d), the polyhedral particle was composed of Fe, Cr, Ni, Zn oxide. At all conditions, a double-layered structure was formed: an outmost layer with Fe-rich oxide and inner layer with Cr-rich oxide. Under the conditions of (b) and (d), Cr-depleted zones were observed in the matrix beneath the Cr-rich layer.
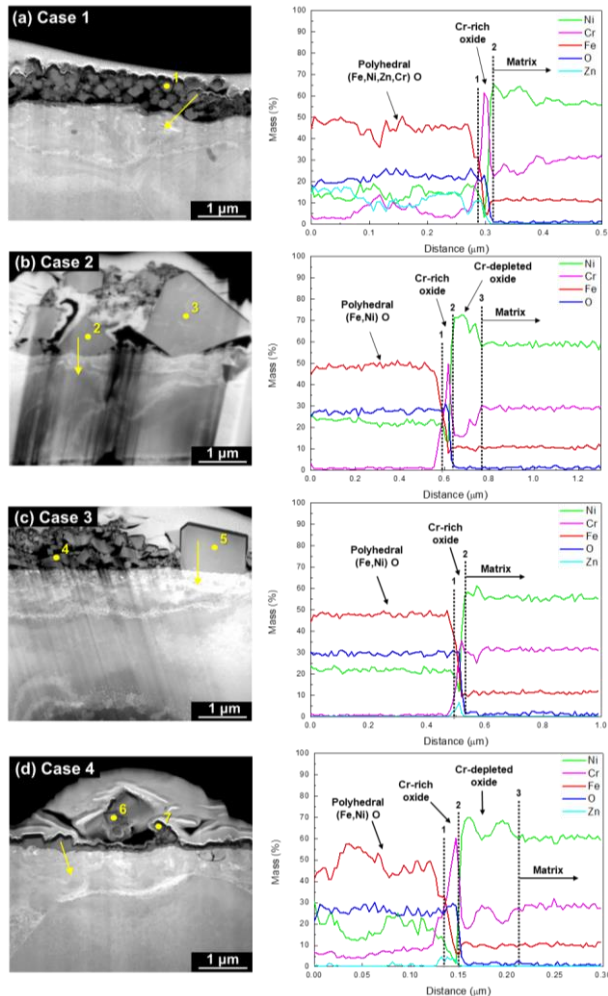
Fig. 3. TEM images and line EDS analyses of cross section of oxide films formed on Alloy 690TT after corrosion tests for 3000 h under the four zinc injection conditions: (a) case 1, (b) case 2, (c) case 3, and (d) case 4.

Table III. Chemical compositions of oxide particles analyzed by EDS (at. %). The points of analysis are indicated in Fig. 3.

Point	Chemical composition (at.%)				
	Ni	Cr	Fe	O	Zn
1	10.42	13.68	20.24	46.99	8.67
2	20.25	0.27	37.30	42.18	-
3	19.91	0.25	37.15	42.69	-
4	4.69	2.02	34.17	52.33	6.79
5	14.62	0.18	32.33	52.20	0.67
6	11.40	12.57	16.78	55.32	3.93
7	13.33	12.98	18.48	53.58	1.63

In the future, the general corrosion rate of Alloy 690TT will be evaluated by using the chemical descaling methods according to ASTM G1-03. In addition, the mechanism on the effect of zinc injection timing on the oxide formation behavior will be discussed from a thermodynamic viewpoint. X-ray photo spectroscopy (XPS) analysis of oxide films will be also performed soon. These results will be discussed at the oral presentation.

4. Conclusions

This work has investigated the effect of the zinc injection timing on general corrosion behavior of Alloy 690. The main results can be derived:

(1) Under the all zinc injection conditions, all specimens had the polyhedral-shaped oxide particles. Especially, the rod-like oxide particles were additionally observed on the surface of Alloy 690 in the case 3.

(2) Based on the TEM-EDS results, double-layered oxide films was formed on Alloy 690TT under all conditions: an outmost layer with Fe-rich oxide containing of Ni, Cr, and Zn and an inner layer with Cr-rich oxide containing of Ni, Fe, and Zn.

(3) The size and density of oxide particles were significantly changed with zinc injection timing. The density and size of particles formed on the surface of test specimens was ranked in the following order: case 2 > case 4 > case 3 > case 1.

(4) Based on the SEM micrographs, it is expected that the general corrosion resistance of Alloy 690 would be ranked in the following order: case 1 > case 3 > case 4 > case 2.

Acknowledgements

REFERENCES

[1] W.A Byers., and J. Deshon, structure and chemistry of PWR crud, in: proceedings of the International Conference on Water Chemistry of Nuclear Reactor Systems. San Francisco, USA, pp.1722-1731, 2004.

[2] J. Deshon, D. Hussey., B. Kendrick, J. McGurk, J. Secker, M. Short, Pressurized water reactor fuel crud and corrosion modeling, JOM-J. Miner. Met. Mater. Soc., Vol. 63, No. 8, pp. 64-72, 2011.

[3] R.W Steahle, J.A. Gorman, Corrosion, Vol. 59, pp. 931-994, 2003.

[4] I. Betova, M. Bojinov, P. Kinnunen, T.Saario, Zn injection in Pressurized Water Reactors-Laboratory Tests, Field Experience and Modelling, (Report), VTT-R-05511-11, 2011.

[5] S.H. Jeon, Journal of Nuclear Materials, Vol. 485, pp. 113-121, 2017.

[6] Q. Peng, J. Hou, K, Sakaguchi, Y. Takeda, T. Shoji, Electrochim, Acta., Vol. 56, pp. 8375-8386, 2011.

[7] J. Xu, T. Shoji, C.H. Jang, Corros. Sci., Vol. 97, pp. 115-125, 2015.

[8] EPRI, Overview Report on Zinc Addition in PWRs, Palo Alto, CA:1001020, 2006.